Computers and Concrete, Vol. 8, No. 1 (2011) 1-22
DOI: http://dx.doi.org/10.12989/cac.2011.8.1.001

A numerical tension-stiffening model for ultra high strength fiber-reinforced concrete beams

Chaekuk Na and Hyo-Gyoung Kwak*

Department of Civil and Environmental Engineering, Korea Advanced Institute of Science and Technology, 335 Gwahak-ro, Yuseong-gu, Daejeon, Korea, 305-701

(Received July 30, 2009, Accepted December 3, 2009)

Abstract. A numerical model that can simulate the nonlinear behavior of ultra high strength fiber-reinforced concrete (UHSFRC) structures subject to monotonic loadings is introduced. Since engineering material properties of UHSFRC are remarkably different from those of normal strength concrete and engineered cementitious composite, classification of the mechanical characteristics related to the biaxial behavior of UHSFRC, from the designation of the basic material properties such as the uniaxial stress-strain relationship of UHSFRC to consideration of the bond stress-slip between the reinforcement and surrounding concrete with fiber, is conducted in this paper in order to make possible accurate simulation of the cracking behavior in UHSFRC structures. Based on the concept of the equivalent uniaxial strain, constitutive relationships of UHSFRC are presented in the axes of orthotropy which coincide with the principal axes of the total strain and rotate according to the loading history. This paper introduces a criterion to simulate the tension-stiffening effect on the basis of the force equilibriums, compatibility conditions, and bond stress-slip relationship in an idealized axial member and its efficiency is validated by comparison with available experimental data. Finally, the applicability of the proposed numerical model is established through correlation studies between analytical and experimental results for idealized UHSFRC beams.

Keywords: ultra high performance concrete (UHPC); steel fiber-reinforced concrete (SFRC); tension-stiffening model; tensile properties; finite element analysis.

1. Introduction

Rapid increase in the number of construction projects involving long-span bridges and high-rise buildings has necessitated the development of construction materials possessing increased strength. Concrete, which has become one of the most important construction materials and is widely used in many types of engineering structures, is not an exception. Following the introduction of normal strength concrete, its strength has been continuously increased; however, the brittleness of concrete is proportion to the increase in compressive strength. To overcome the brittleness of concrete, engineered cementitious composite (ECC) has been developed by adding various types of fibers at different volume fractions to the concrete matrix (Li 1998). ECC's tensile strain hardening behavior has a capacity in the range of 3% to 7%; however, the compressive strength has not been increased compared to normal concrete. In an effort to improve the strength and toughness of concrete, ultra high strength concrete with steel fibers added in the concrete matrix, namely, ultra high strength

* Corresponding author, Professor, E-mail: khg@kaist.ac.kr

fiber-reinforced concrete (UHSFRC), has been developed by many researchers.

In order to use UHSFRC as a construction material, however, the structural behavior of UHSFRC members as well as the material properties of UHSFRC itself must be verified. In this regard, numerous relevant experimental studies have been conducted (Kölle *et al.* 2004, Mansur *et al.* 1999). Within the framework of developing advanced design and analysis methods for UHSFRC structures, experimental study is required, as experiments provide a firm basis for design equations and also supply basic information for numerical analyses, such as material properties. In addition, the results of numerical analyses should be evaluated through comparison with results of experiment involving full-scale models of the structural sub-assemblages or the entire structures.

The development of reliable analytical models can reduce the number of required test specimens for the solution of a given problem (Kwak and Kim 2001, Kwak and Na 2007). This is of notable importance given that tests are time-consuming and costly and often do not simulate exactly the loading and support conditions of the actual structure. Nevertheless, very little work has been carried out on the structural behavior of UHSFRC systems on the basis of finite element analyses (Foster *et al.* 2006), because of the computational effort involved and insufficient knowledge of the material behavior of UHSFRC under biaxial stress state. With the recognition that many of the material models for biaxial loading have yet to be fully verified so far (Demeke and Tegos 1994, Hussein and Marzouk 2000, Kölle *et al.* 2004), one of the aims of this paper is to address some model selection issues in the numerical analyses of UHSFRC structures, in particular, with regard to the strength of the reinforcing steel and the tension-stiffening effect in concrete.

This paper introduces an improved numerical tension-stiffening model of UHSFRC members on the basis of the force equilibriums, compatibility conditions, and simplified bond stress-slip relationship. The introduced model is idealized with four boundary values corresponding to the stabilized crack strain, the steel and fiber yielding strains, and the pull-out strain, respectively. The use of the tension-stiffening model makes it possible to accurately simulate the post-cracking behavior of UHSFRC members dominantly affected by the tension-stiffening effect rather than normal strength concrete members. Finally, the introduced numerical model is validated by comparison with test results for idealized UHSFRC beams, and additional parametric studies are conducted to review the structural behavior of UHSFRC beams according to the tension-stiffening effect and the change in material properties.

2. Material properties

2.1 Concrete

The uniaxial stress-strain curves of normal strength concrete have been proposed on the basis of experimental studies of a numerous idealized relationships. Likewise, in the cases of steel fiber-reinforced concrete, experimental studies have been conducted to describe the stress-strain relationship of corresponding concrete (Hussein and Marzouk 2000, Kölle *et al.* 2004, Mansur *et al.* 1999). A typical normalized compressive stress-strain relationship of SFRC is shown in Fig. 1. An increase of the compressive strength accompanies a rapid decrease of ductility in the strain softening region; however, this brittleness has been overcome by adding fibers to the concrete, as this increases both the ductility of concrete and its fatigue strength (Ezeldin and Balaguru 1992). In general, improvement of the ductility of concrete has made it possible to develop higher strength concrete

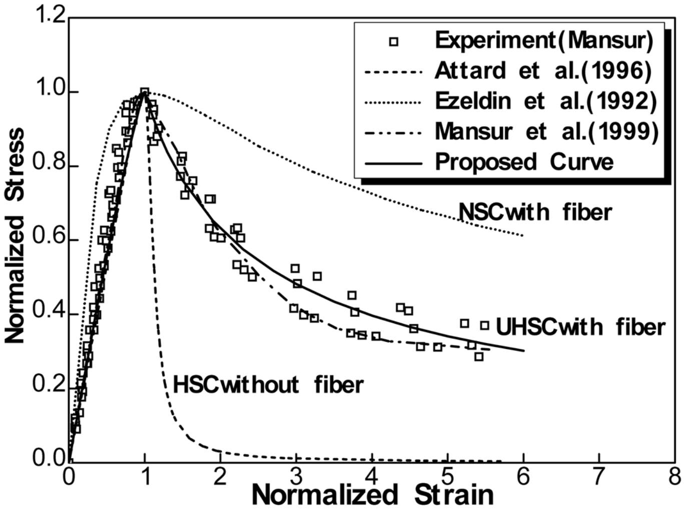

Fig. 1 Normalized compressive stress-strain relationship of UHSFRC

such as UHSFRC and has facilitated practical application of UHSFRC structures.

In describing the uniaxial compressive stress-strain behavior of UHSFRC, more attention must be given to the strain softening region. Many empirical equations of NSC were proposed to define the stress-strain relationship, and each general relationship was agreed well with the experimental test (Hognestad 1951); since the principal variable was the compressive strength of concrete specimen. However, unlike NSC, the compressive behavior of UHSFRC, which depends to fiber content and specimen dimension, is difficult to choose a specific general stress-strain relationship. Upon this background, because test data are not sufficient to suggest a unique compressive stress-strain relationship, this paper introduces the stress-strain relationship given in Eq. (1), wherein the ascending branch represents a similar equation to that popularly used for NSC (Hognestad 1951) and the descending branch is a regression equation determined on the basis of experimental data (Mansur *et al.* 1999). In Fig. 1, the stress-strain relationship of NSC with fiber (Ezeldin and Balaguru 1992) and HSC without fiber (Attard and Setunge 1996) are too ductile and brittle, respectively, compare to that of ultra high strength concrete with fiber (Mansur *et al.* 1999).

$$f = \begin{cases} f_c'\{1-(1-\varepsilon/\varepsilon_c)^{k_1}\} & 0 \le \varepsilon \le \varepsilon_c \\ f_c'\left\{\dfrac{e^{-\sqrt{\varepsilon/\varepsilon_c - k_2}}}{k_2} + k_3\right\} & \varepsilon \ge \varepsilon_c \end{cases} \tag{1}$$

where f_c' is the compressive strength of UHSFRC, ε_c is the peak strain corresponding to f_c', and $E_c = 3.840\sqrt{f_c'}$ represents the initial modulus of elasticity introduced by Graybeal (2007) for all range of concrete strength. In general, the shape function $k_1 = ln(1-\eta)/ln\{1-\eta/(E_c\varepsilon_c/f_c')\}$ can be determined by assuming the secant ratio $\eta = f/f_c'$, and the material parameters of $k_2 = 0.65$, $k_3 = 0.15$, required to define the descending branch, can be determined through the correlation between the regressive curve and the experimental data of Mansur *et al.* (1999).

With a uniaxial stress-strain relationship of concrete, the material behavior of concrete under

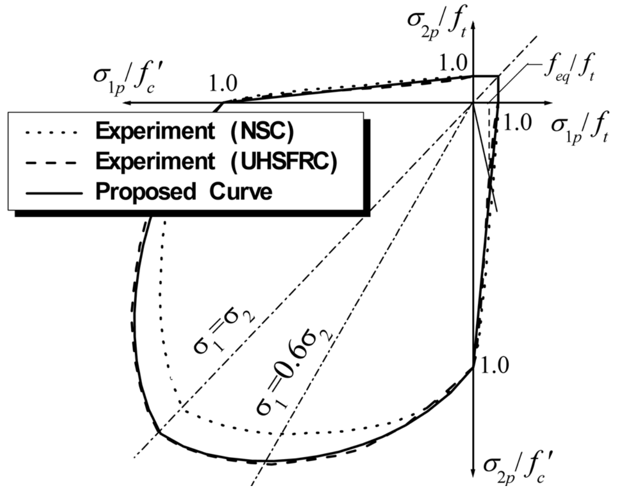

Fig. 2 Biaxial strength failure envelope of UHSFRC

biaxial loading needs to be defined, because the strength characteristic and stress-strain behavior of concrete are somewhat different from those of concrete under uniaxial loading due to the effects of Poisson's ratio and micro crack confinement (Kwak and Na 2007). To simulate the change of material properties according to the stress state, it is thus necessary to define the biaxial strength envelope. As conducted for normal strength concrete, corresponding experimental studies have also been performed for UHSFRC (Demeke and Tegos 1994, Hussein and Marzouk 2000, Kölle *et al.* 2004). Fig. 2 shows the biaxial strength failure envelope of UHSFRC introduced in this paper along with that of NSC for comparison.

The accompanying equation for the failure envelope has been designed on the basis of Kölle's experimental data for the compression-compression region and Demeke's and Hussein's experimental data for the compression-tension and the tension-tension region, respectively. Some experimental results show that the compressive-compressive behavior of UHSFRC always depend on the fiber content; however, some experimental results show the opposite behavior. Differently from both equations defined in the tension-tension region and the compression-tension region, which are similar to those introduced by Kupfer's experimental data for NSC (Kupfer *et al.* 1969), the equation for the failure envelope in the compression-compression region is expressed by

$$f_{2p} = (0.25\xi^3 - 1.25\xi^2 + 1.25\xi + 1)f_c',\ f_{1p} = \xi f_{2p} \tag{2}$$

where $\xi = f_1/f_2$ is the principal stress ratio, and f_{1p} and f_{2p} are the maximum equivalent principal stresses corresponding to the current principal stresses f_1 and f_2, respectively.

After determination of the equivalent concrete compressive strength of f_{1p} and f_{2p} from the biaxial failure surface of UHSFRC, the equivalent uniaxial stress-strain relationship in the compression-compression region, corresponding to the current loading history, is constructed by replacing the compressive strength f_c' in Eq. (1) with the equivalent compressive strength f_{ip}. In the compression-tension and the tension-tension regions, however, the following assumptions are adopted in this paper, because the response of a typical UHSFRC member is considerably more affected by the tensile than the compressive behavior of concrete: (1) failure takes place by cracking when the principal tensile strain exceeds the limit strain; therefore, the tensile behavior of the concrete

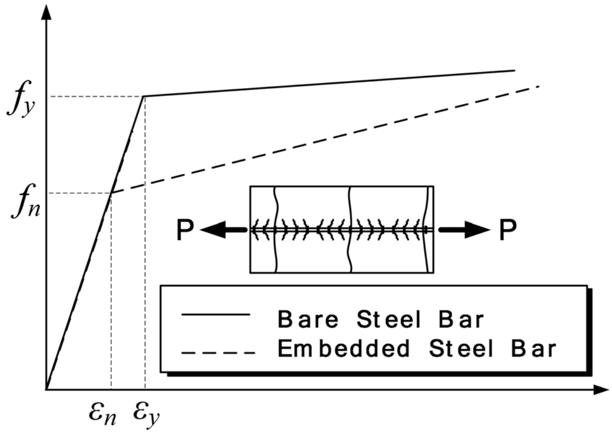

Fig. 3 Stress-strain relationship of steel

dominates the response; (2) the uniaxial tensile strength of concrete f_t is reduced to the value f_{eq}, as shown in Fig. 2, to account for the effect of the compressive stress under a biaxial state; and (3) the concrete stress-strain relationship in compression is the same as that under uniaxial loading and does not change with an increase of the principal tensile stress.

2.2 Steel

The stress-strain curves for steel are generally assumed to be identical in tension and compression. For simplicity in the calculations, it is necessary to idealize a one-dimensional stress-strain curve for the steel element. Normal strength steel is usually assumed to be a linear elastic, linear strain hardening material whose yield stress is f_y (bared steel bar in Fig. 3). As noted in previous studies, however, normal strength steel embedded in a concrete matrix presents different behavior from bared steel bar, because of the bond interaction along the steel bar between adjacent cracks. This means that the averaged yield stress f_n, which is significantly less than f_y, must be used to avoid overestimation of the post-yielding behavior of the reinforced concrete structures in the case of taking the tension-stiffening effect into consideration in the stress-strain relationship of concrete. More details related to the calculation of f_n can be found elsewhere (Kwak and Kim 2004).

3. Tension-stiffening model for UHSFRC

When a symmetrical uncracked RC member is loaded in tension, the tensile force is distributed between the reinforcing steel and the concrete in proportion to their respective stiffness, and cracks in the concrete occur when the stress reaches a value corresponding to the tensile strength of concrete. In a cracked cross-section, all tensile forces are balanced by the steel encased in the concrete matrix only. However, between adjacent cracks, tensile forces are transmitted from the steel to the surrounding concrete by bond forces. This phenomenon is defined as the tension-stiffening effect, and the same response also appears in UHSFRC members.

This tension-stiffening effect can be adequately taken into account by the increased average stiffness of an element. An increase of tensile stiffness of concrete can be accomplished by using

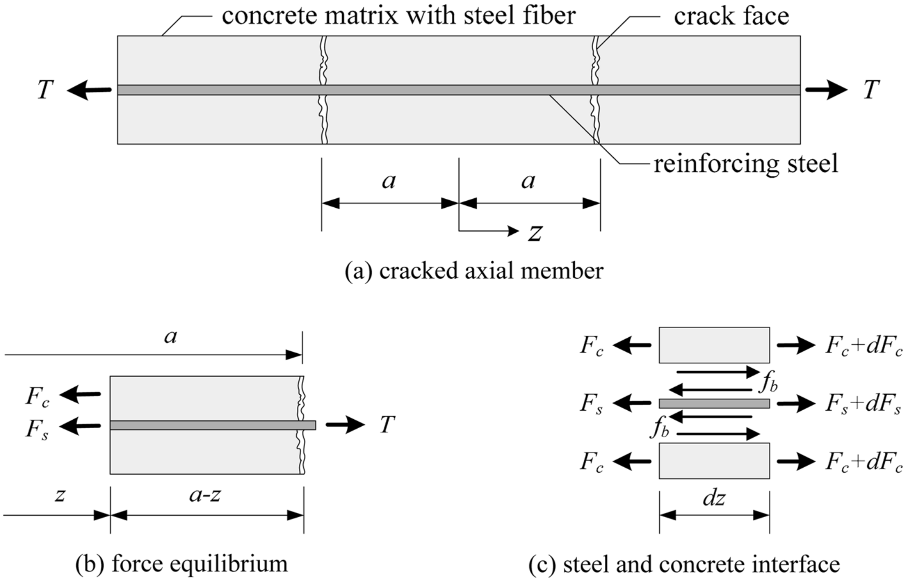

Fig. 4 Descriptions for a cracked UHSFRC axial member

a stress-strain relationship that includes a descending branch in the tension region. In this paper, based on the force equilibriums, compatibility conditions, and bond stress-slip relationship between the reinforcement and the surrounding concrete in an axial tension member, a descending branch to define the post-cracking stress-strain relationship of concrete is proposed. Additionally, the bonding resistance between the steel fibers and the concrete matrix in UHSFRC is also taken into consideration, because steel fiber-reinforced concrete can exhibit significant post-cracking tensile resistance at cracks, depending on the type and dosage of the steel fiber used.

3.1 Force equilibrium

As was verified from experiments (Bischoff 2003, Kölle *et al.* 2004), the use of steel fibers can improve the bond and reduce crack spacing. A cracked axial UHSFRC member subject to a direct tensile force T is shown in Fig. 4(a). A part of the member bounded by adjacent cracks with a crack spacing of $2a$ can be taken as the free body diagram.

Since the applied direct tensile force T is carried partly by the concrete matrix (F_c) and partly by the reinforcing steel (F_s), the following force equilibrium equation can be obtained (see Fig. 4(b))

$$T = F_c + F_s \tag{3}$$

The two force components carried by the concrete matrix and the reinforcing steel can be expressed by

$$F_c = A_c E_c \varepsilon_c = A_c E_c \frac{du_c}{dz} \tag{4a}$$

$$F_s = A_s E_s \varepsilon_s = A_s E_s \frac{du_s}{dz} \tag{4b}$$

where E, ε, u and A are the elastic modulus, the strain, the deformation, and the sectional area corresponding to each material of the concrete matrix (subscript c) and the reinforcing steel (subscript s), respectively.

Reinforcing bars transfer tensile stresses to the concrete matrix through the bond stresses along the surface between the reinforcements and the surrounding concrete. Therefore, an infinitesimal element of the length dz is taken out from the intact concrete between adjacent cracks to obtain the equilibrium equations for the concrete matrix and the reinforcing steel. Fig. 4(c) presents the free body diagram at the steel and concrete interface. The following equilibrium equations of force deviation for the steel and concrete, which are expressed in terms of the bond parameters, can be obtained

$$\frac{dF_c}{dz} = -pmf_b \tag{5a}$$

$$\frac{dF_s}{dz} = +pmf_b \tag{5b}$$

where p is the perimeter of the reinforcing bar, m is the number of reinforcing bars placed, and f_b is the bond stress at the steel-concrete interface.

3.2 Bond-slip behavior

Since the bond slip Δ at the steel-concrete interface is defined by the relative displacement between the reinforcing steel and concrete matrix ($\Delta = u_s - u_c$), substitution of Eqs. (4) and (5) into the second order differential equation of the bond slip leads to Eq. (6), if the linear bond stress-slip relationship given by $f_b = E_b\Delta$ is assumed

$$\frac{d^2\Delta}{dz^2} - k^2\Delta = 0 \tag{6}$$

where $k^2 = (pmE_b/A_sE_s) \cdot (1+n\rho)$, E_b= the slip modulus, $n = E_s/E_c$, and $\rho = A_s/A_c$. In particular, $n\rho$ means the area parameter and k^{-1} represents the characteristic length (Gupta and Maestrini 1990).

The general solution to Eq. (6) given by $\Delta = C_1 \sinh kz$ can be solved from the boundary conditions: (1) the slip should be zero at the center (z = 0) between crack faces, and (2) the slips at both crack faces must be the same because of the symmetry ($\Delta(-z) = -\Delta(z)$). Integration of Eq. (5) after substituting the obtained general solution leads to the following expression for the steel force F_S

$$F_s = \frac{pmE_bC_1}{k}\cosh kz + C_3 \tag{7}$$

where the constant of integration $C_3 = (T - F_f) - (pmE_bC_1/k)$ is obtained from the boundary condition at the crack surface ($F_s = T - F_f$ at $z = a$), because the steel fiber of the concrete matrix resists the tensile force (F_f) at the crack face, as shown in Fig. 5. The general solutions for the concrete and steel forces can be written as

$$F_c = F_f + \frac{pmE_bC_1}{k}(\cosh ka - \cosh kz) \tag{8a}$$

$$F_s = (T - F_f) - \frac{pmE_bC_1}{k}(\cosh ka - \cosh kz) \tag{8b}$$

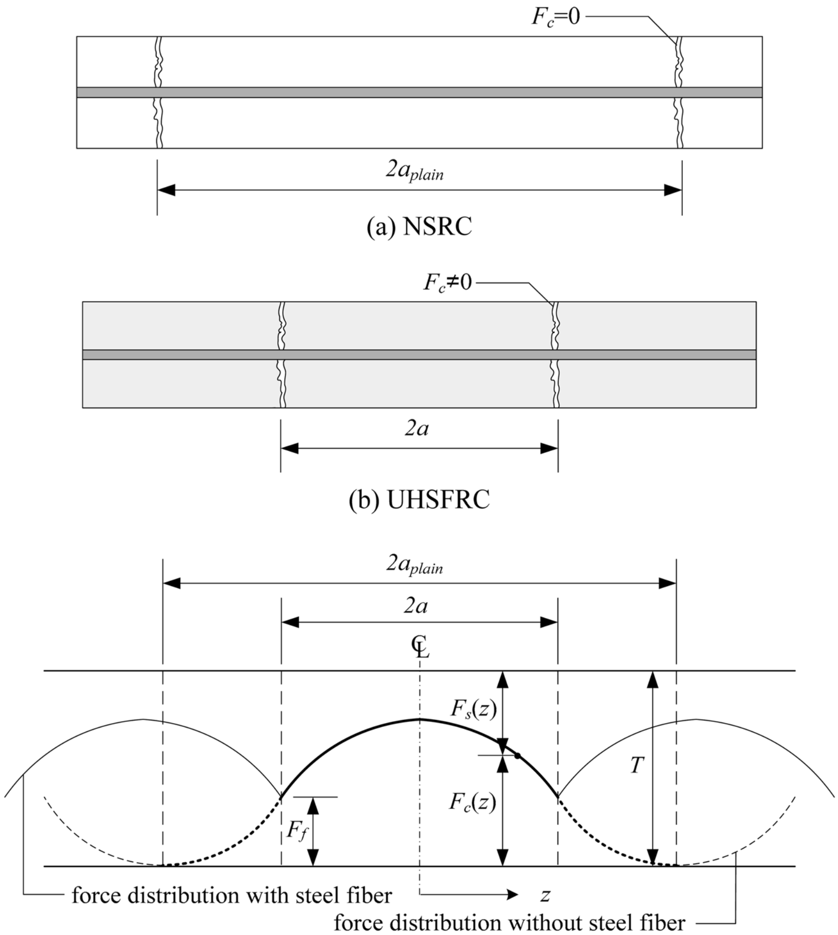

(c) force distribution between NSRC and UHSFRC

Fig. 5 Cracks and forces distribution between adjacent cracks

where F_f denotes the tensile force carried by the steel fiber in UHSFRC at the crack face.

If the resisting force by the steel fiber at the crack face (F_f) is assumed to be proportional to the concrete force F_c at the center ($z = 0$), that is, $F_f = \alpha F_c(0)$ (Bischoff 2003), then the following relationship for F_f can be obtained, where α is a coefficient related to the steel fiber and concrete properties and can be determined from the force equilibrium. Noted that α must be larger than or equal to zero ($\alpha \geq 0$).

$$F_f = \frac{\alpha}{1-\alpha} \cdot \frac{pmE_bC_1}{k}(\cosh ka - 1) \tag{9}$$

In advance, the displacements of concrete and steel along the reinforcement can be calculated from Eqs. (4), (8) and (9) through integration with respect to the principal direction, z.

$$u_c = 1 + n\rho \cdot \frac{c_1}{1+n\rho}\left\{\frac{kz}{1-\alpha}(\cosh ka - \alpha) - \sinh kz\right\} \tag{10a}$$

$$u_s = \frac{Tz}{A_s E_s} - \frac{c_1}{1+n\rho}\left\{\frac{kz}{1-\alpha}(\cosh ka - \alpha) - \sinh kz\right\} \tag{10b}$$

in which $C_1 = (T/A_s E_s)(1-\alpha)/\{k(\cosh ka - \alpha)\}$ is uniquely determined from the two relationships of $\Delta = u_s - u_c$ and $\Delta = C_1 \sinh kz$.

3.3 Tension-stiffening model

On the basis of the obtained equations for the displacements, the descending branch in the tension region of the concrete stress-strain relationship can be determined. To take into account the tension-stiffening behavior, the average behavior of UHSFRC needs to be defined with the effective tensile stress (σ_{cm}) and the corresponding average strain ($\varepsilon_{sm} = \varepsilon_{cm}$) in the concrete matrix. First, the equilibrium equation in Eq. (3) can be rearranged as

$$T = A_c \sigma_{cm} + A_s E_s \varepsilon_{sm} \tag{11}$$

These two values of σ_{cm} and $\varepsilon_{sm}(= \varepsilon_{cm})$ can be obtained from Eq. (10).

$$\varepsilon_{sm} = \frac{u_s(a)}{a} = \frac{T}{A_s E_s} \cdot \frac{1}{1+n\rho}\left\{n\rho + \frac{(1-\alpha)\sinh ka}{ka(\cosh ka - \alpha)}\right\} \tag{12a}$$

$$\sigma_{cm} = \frac{T}{A_s} \cdot \frac{1}{1+n\rho}\left\{1 - \frac{(1-\alpha)\sinh ka}{ka(\cosh ka - \alpha)}\right\} \tag{12b}$$

The maximum tensile force in the concrete matrix occurs at $z = 0$, and the corresponding concrete stress is $\sigma_{c,max} = F_{c,max}/A_c$; that is, the maximum tensile stress in the concrete is directly proportional to the applied principal tensile force T. Accordingly, $\sigma_{c,max}$ converges to the tensile strength of the concrete (f_t) as the applied tensile force T increases. At that point, a new crack will be formed at $z = 0$, and the corresponding crack strain will be $\varepsilon_{crack} = \sigma_{c,max}/E_c$.

$$\sigma_{c,max} = \frac{T}{A_s} \cdot \frac{1}{1+n\rho}\left(1 - \frac{1-\alpha}{\cosh ka - \alpha}\right) \tag{13a}$$

$$\varepsilon_{crack} = \frac{T}{A_c E_c} \cdot \frac{1}{1+n\rho}\left\{1 - \frac{1-\alpha}{\cosh ka - \alpha}\right\} \tag{13b}$$

After eliminates T from Eqs. (12) and (13), they are rewritten in a non-dimensional form.

$$\frac{\sigma_{cm}}{\sigma_{c,max}} = \frac{1 - \dfrac{(1-\alpha)\sinh ka}{ka(\cosh ka - \alpha)}}{1 - \dfrac{1-\alpha}{\cosh ka - \alpha}} \tag{14a}$$

$$\frac{\varepsilon_{cm}}{\varepsilon_{crack}} = \frac{1 + \dfrac{(1-\alpha)\sinh ka}{n\rho ka(\cosh ka - \alpha)}}{1 - \dfrac{1-\alpha}{\cosh ka - \alpha}} \tag{14b}$$

In Eq. (14), the crack spacing $2a$ is the same as the specimen length (L), and becomes progressively shorter, $L/2$, $L/4$, ... and so on. Finally, $\sigma_{cm}/\sigma_{c,max}$ converges to the value of 2/3 as the parameter ka related to the crack spacing approaches zero. However, the actual crack spacing is not narrowed any further but remains constant after reaching a certain value. The experimental study indicated that the number of cracks is stabilized when the average strain is about 0.001 in an axial normal strength reinforced concrete (NSRC) member (Rizkalla and Hwang 1984). An experimental study for a UHSFRC member was also conducted and it was reported that the average crack width (w_m) and the average crack spacing (s_m) are roughly half those obtained in NSRC members (Lorrain *et al.* 1998). This means that the stabilized strain of the UHSFRC member converges to 0.001, as is the case for the NSRC member, as given by the relationship $w_m = s_m \times \varepsilon_m$, representing the average crack width = the average crack spacing × the average strain. Accordingly, with the assumption that the linear bond stress-slip relationship holds, Eq. (14) can be available up to $\varepsilon_{cm} = 0.001$ (point A in Fig. 6).

Further deformation leads to yielding of the reinforcing steel, followed by an increase of the slip while maintaining a plateau $f_b = \tau_b$. For continued increase of the slip, the bond stress decreases linearly to the value of the ultimate frictional bond resistance. In the case of constant bond stress and yielding of the reinforcing steel, the tensile force carried by the concrete matrix and reinforcing steel can be calculated from Eq. (5) with the appropriate boundary conditions of the steel fiber force F_f at the crack face, given in Fig. 5(c).

$$F_c = F_f + pm\,\tau_b(a-z) \tag{15a}$$

$$F_c = (T-F_f) - pm\,\tau_b(a-z) \tag{15b}$$

The assumed force component for the steel fiber ($F_f = \alpha F_c(0)$) makes it possible to calculate the concrete and the steel forces. From Eqs. (4) and (15), the displacements of the concrete and the steel can be expressed as follows

$$u_c = n\rho\frac{pm\,\tau_b z}{A_s E_s}\left(\frac{a}{1-\alpha}-\frac{1}{2}z\right) \tag{16a}$$

$$u_s = \frac{Tz}{A_s E_s} - \frac{pm\,\tau_b z}{A_s E_s}\left(\frac{a}{1-\alpha}-\frac{1}{2}z\right) \tag{16b}$$

Furthermore, the average strain in the reinforcing steel ε_{sm} can be obtained by differentiating u_s with respect to z at the crack face. Accordingly, the effective tensile stress of concrete can be calculated from Eq. (11) with the average strain in the reinforcing steel ε_{sm}.

$$\varepsilon_{sm} = \frac{u_s(a)}{a} = \frac{T}{A_s E_s}\left\{T - \frac{pm\,\tau_b a}{2}\cdot\frac{1+\alpha}{1-\alpha}\right\} \tag{17a}$$

$$\sigma_{cm} = \frac{1}{A}\cdot\frac{pm\,\tau_b a}{2}\cdot\frac{1+\alpha}{1-\alpha} \tag{17b}$$

The maximum tensile force in the concrete matrix occurs at $z = 0$ ($F_{c,max}$) and can be obtained from Eq. (15) as:

$$F_{c,max} = \frac{pm\tau_b a}{2} \cdot \frac{2}{1-\alpha} \tag{18}$$

The non-dimensional parametric equations, as applied in the case of linear bond stress-slip relationship, are determined as follows (point B in Fig. 6)

$$\frac{\sigma_{cm}}{\sigma_{c,max}} = \frac{1+\alpha}{2} \tag{19a}$$

$$\frac{\varepsilon_{cm}}{\varepsilon_{crack}} = \frac{1-\alpha}{n\rho}\left(\frac{T}{pm\tau_b a} - \frac{1}{2} \cdot \frac{1+\alpha}{1-\alpha}\right) \tag{19b}$$

where the corresponding concrete stress and strain are $\sigma_{c,max} = F_{c,max}/A_c$ and $\varepsilon_{crack} = \sigma_{c,max}/E_c$, respectively, and the principal tensile force T is given by $T = A_s f_y + \alpha A_c f_t$ at the crack face. The coefficient $\alpha = 0$ corresponding to normal strength concrete without steel fibers indicates $\sigma_c/\sigma_{c,max} = 1/2$, which agrees with the previous studies (Gupta and Maestrini 1990, Kwak and Kim 2004).

The coefficient α is determined from Eq. (20), representing the force equilibrium in an axial member composed of the ultra high strength concrete matrix and reinforcing steel at two typical sections located at the center of the specimen ($z = 0$) and at the crack face ($z = a$), respectively.

$$T = F_s(0) + F_c(0) = F_s(a) + F_c(a) \tag{20}$$

where $F_c(0) = f_t A_c$, $F_s(0) = T - pm\tau_b a/(1-\alpha)$ are the concrete and steel forces at the center, respectively, and $F_c(a) = \alpha f_t A_c$ is the steel fiber force at the crack face, which is proportional to the concrete force at the center, $F_s(a) = T - pm\tau_b a \cdot \alpha/(1-\alpha)$ is the steel force at the crack face when the reinforcing steel yields. Hence, the coefficient α can be expressed in terms of the concrete and bond parameters.

$$\alpha = 1 - \frac{pm\tau_b a}{f_t A_c} \geq 0 \tag{21}$$

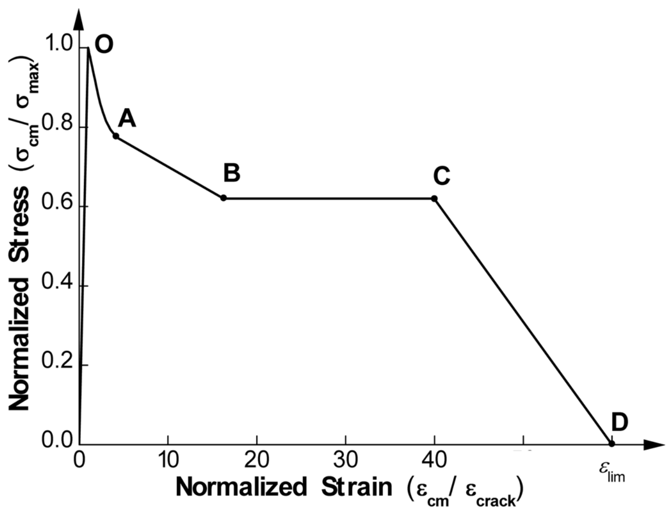

Fig. 6 Effective concrete tensile stress-strain relationship

Accordingly, the tensile force carried by the steel fiber at the crack face, which is assumed to be proportional to the concrete force at center ($F_f = \alpha F_c(0)$), remains constant even after yielding of the reinforcing steel, while the average steel strain is rapidly enlarged. An increase in the average steel strain at the post-yielding stage will continue until the elongation in the steel fiber ($\Delta l_f = (f_{y,f}/E_f) \cdot l_f$) equates with the average crack width (w_m), where l_f and $f_{y,f}$ represent the length and its yielding strength of the steel fiber, respectively. Hence, from the relationship $w_m = s_m \times \varepsilon_m$ (Lorrain *et al.* 1998), the average tensile strain for this critical condition, in which the normalized concrete stress $\sigma_{cm}/\sigma_{c,max} = (1+\alpha)/2$ maintains a uniform value without any change from that defined by point B in Fig. 6, can be determined (point C in Fig. 6).

Finally, the limit average strain ε_{lim} in the reinforcing steel needs to be defined. SETRA (2002) indicates that the effective tensile stress of concrete disappears when the crack width ($w_m = \varepsilon_{lim} \cdot l_c$) reaches 1/4 of the length of the steel fiber. Therefore, the limit average strain (ε_{lim}) in the reinforcing steel can be expressed by the length of steel fiber (l_f) and the characteristic length (l_c), where $l_f = 2h/3$ for a rectangular section with h = height of the section (point D in Fig. 6).

$$\varepsilon_{lim} = l_f/4l_c \tag{22}$$

4. Solution procedure

Based on the material models of concrete including the tension-stiffening effect and reinforcing steel defined previously to present the material nonlinearity, a finite element formulation was conducted. The distributed steel model was adopted, because the reinforcement is uniformly distributed over the concrete matrix with a particular orientation angle in an element. The steel fiber effect to enhance the stiffness at post-cracking loading stage is indirectly taken into consideration through the proposed tension-stiffening model. Accordingly, two-dimensional plane element is used for all elements, since it can simulate the biaxial cracking behavior more effectively compare to one-dimensional layered beam element.

To simulate the stress state of the concrete under biaxial loading, the orthotropic model was adopted in this paper for its simplicity and computational efficiency. With reference to the principal axes of orthotropy, the incremental constitutive relationship can be expressed by

$$\begin{Bmatrix} d\sigma_1 \\ d\sigma_2 \\ d\sigma_3 \end{Bmatrix} = [D]_{LO} \begin{Bmatrix} d\varepsilon_1 \\ d\varepsilon_2 \\ d\varepsilon_3 \end{Bmatrix} \tag{23}$$

$$[D]_{LO} = \frac{1}{1-v^2} \begin{bmatrix} E_1 & v\sqrt{E_1 E_2} & 0 \\ v\sqrt{E_1 E_2} & E_2 & 0 \\ 0 & 0 & (1-v^2)G \end{bmatrix} \tag{24}$$

where $(1-v^2)G = 0.25(E_1 + E_2 - 2v\sqrt{E_1 E_2})$, E_1, and E_2 are the secant moduli of the elasticity in the direction of the axes of orthotropy, which are oriented perpendicular and parallel to the crack direction. Additionally, G is the shear modulus of the elasticity and v is Poisson's ratio.

As cracks progress, changes in the crack direction are simulated using the rotating crack model with the smeared crack model, it is assumed that a crack forms in a direction perpendicular to the principal strain when the principal tensile strain exceeds the cracking strain ε_o. Since the material matrix is defined with reference to the principal strain direction, it must be transformed to the global coordinate system before all element stiffness matrixes can be assembled. This is accomplished by the following transformation

$$[D]_{GL} = [T]^T [D]_{LO} [T] \tag{25}$$

where $tan2\theta = \gamma_{xy}/(\varepsilon_x - \varepsilon_y)$, θ is the angle between the direction normal to the crack and the global x-direction, and $[T]$ is a transformation matrix.

The reinforcing bars embedded in the concrete element are replaced by an equivalent steel element. Since the equivalent steel element has uniaxial properties in the direction parallel to the axis of the reinforcing bars, the constitutive material matrix takes the simple form:

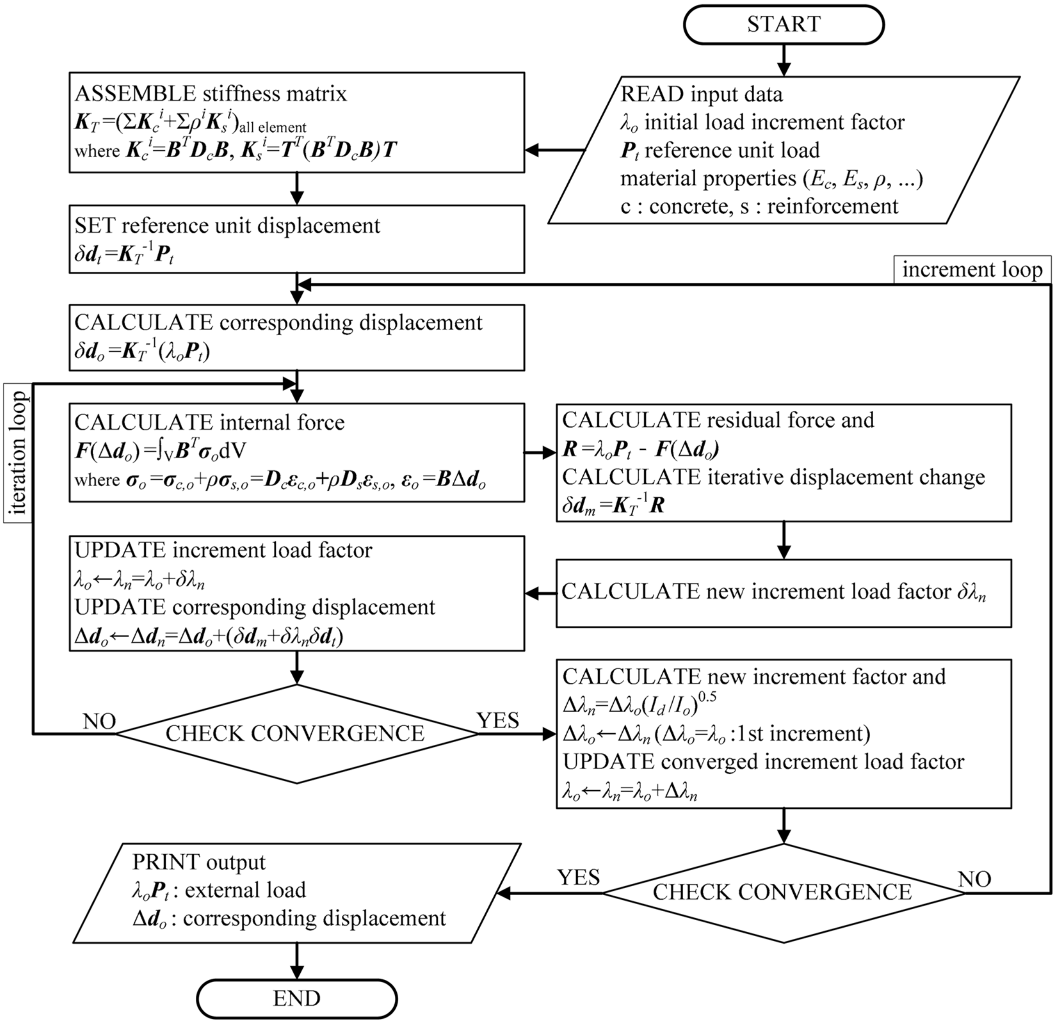

Fig. 7 Flowchart for solution procedure

$$[D_s]_{LO} = \begin{bmatrix} \rho_i E_{si} & 0 & 0 \\ 0 & 0 & 0 \\ 0 & 0 & 0 \end{bmatrix} \tag{26}$$

The stiffness matrix of the composite reinforced concrete arrived at by the superposition of the concrete and reinforcing steel stiffness matrix can be expressed as Eq. (27), where n is the number of steel elements embedded in the concrete element.

$$[K]_{el} = [K_c]_{el} + \sum_{i=1}^{n} [K_s]_{i,el} = \int_V [B]^T \left\{ [D_c]_{GL} + \sum_{i=1}^{n} [D_s]_{i,GL} \right\} [B] dV \tag{27}$$

The arc-length method (Crisfield 1991) has recently been adopted as a solution scheme for the material nonlinear analysis of UHSFRC structures displaying strength degradation after yielding of steel. All of the remaining procedures, from the construction of the element stiffness matrix to the convergence check, are identical to those used in a classical nonlinear analysis of RC structures. A summary of the nonlinear solution algorithm is presented in Fig. 7, and more details of arc-length method can be found elsewhere (Crisfield 1991).

5. Verification of tension-stiffening model

To verify the efficiency of the introduced tension-stiffening model, the cracking behaviors of tension members subject to direct tensile force were analyzed. Two different tension members, which are composed of high strength concrete and ultra high strength fiber-reinforced concrete tested by Bischoff (2003) and Jungwirth and Muttoni (2004), respectively, were selected. These two tension members have been the subject of analytical correlation studies (Fields and Bischoff 2004, Redaelli 2006).

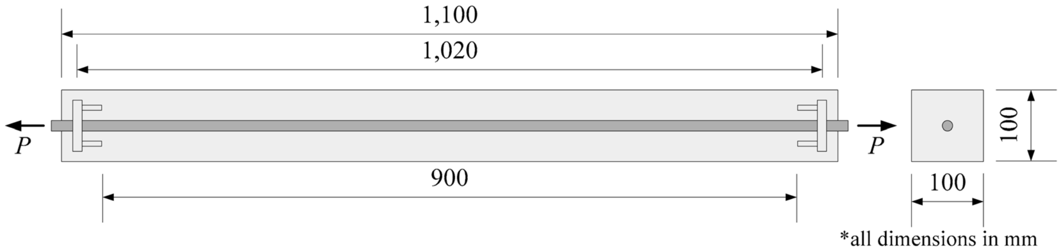

Fig. 8 Configuration of specimen 1

Table 1 Material properties used in specimen 1

Specimen	Concrete properties			Steel properties			
	f_c' (MPa)	f_t(MPa)	E_c^*(GPa)	f_y(MPa)	E_s(GPa)	ρ(%)	ρ_{fiber}(%)
15M	62.4	4.8	33	420.5	202	2.0	0.78
20M				441.7	207	3.0	0.78

*not noted in Bischoff (2003), computed from ACI318 (E_c=3,320 $(f_c')^{1/2}$+6,900)

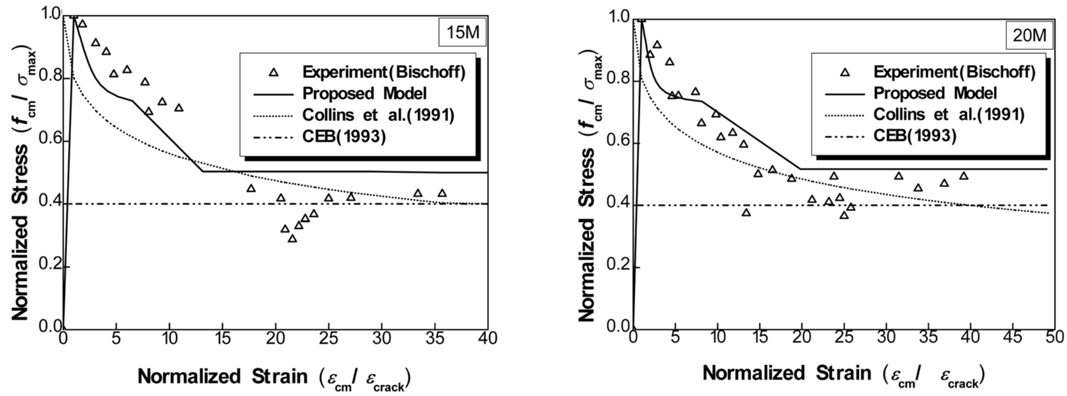

(a) 15M (b) 20M

Fig. 9 Normalized stress-strain relationship

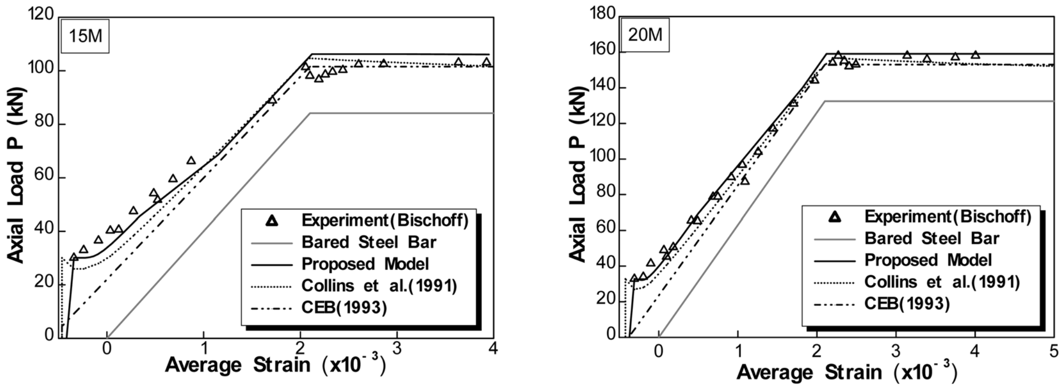

(a) 15M (b) 20M

Fig. 10 Member response with tension-stiffening effect

The first specimen (specimen 1), as shown in Fig. 8, is a specimen with a square cross section dimension of 100 mm × 100 mm and is reinforced with either a single 15M or 20M bar, corresponding to a steel ratio of 2% and 3%, respectively. The material properties of the test specimen are summarized in Table 1, and more details related to the experimental study can be found elsewhere (Bischoff 2003).

Figs. 9 and 10 show the cracking responses for the bonded members. Since this study did not take into account the member shortening caused by shrinkage, the initial offset in the strain distribution induced from shrinkage deformation of the concrete matrix has been subtracted from the original experimental data. Fig. 9 shows the relationship between the normalized stress and the normalized strain, and Fig. 10 represents the corresponding relationship between the applied axial load and the average axial strain.

The comparisons of the experimental and analytical results show that the introduced tension-stiffening model presents improved cracking behavior through all the loading stages. CEB model (1993) recommends a constant value of 0.4 for the normalized stress at the post-cracking stage regardless of the magnitude of the corresponding strain; therefore, the cracking load seems lower

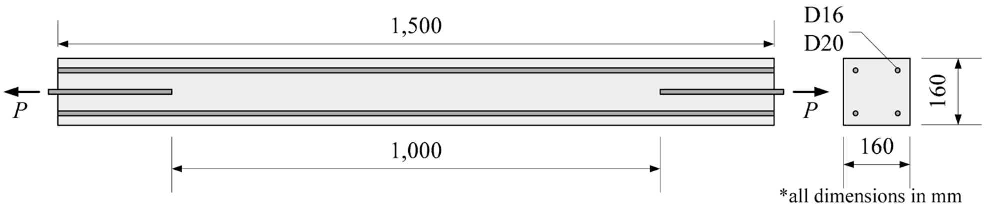

Fig. 11 Configuration of specimen 2

Table 2 Material properties used in specimen 2

Specimen	Concrete properties			Steel properties			
	f_c' *(MPa)	f_t(MPa)	E_c(GPa)	f_y(MPa)	E_s(GPa)	ρ(%)	ρ_{fiber}(%)
2.5%	146	8.9	63	556	200	3.14	2.5
4.1%						4.94	4.1

*not noted in Jungwirth (2004), conducted from KICT test result (2005)

than that of experimental and analytical model. In addition, during the yielding stage of steel rebar, CEB model cannot fit the experimental results, because it does not take into account the contribution of fibers. Another relationship of Collins and Mitchell (1991), where the normalized stress $= 1/(1+\sqrt{500\varepsilon_m})$ and ε_m equals the average member strain, slightly underestimates the cracking behavior at the initial post-cracking stage. This is attributed to absence of consideration of the bond effect in Collin's model between the concrete matrix and included steel fiber. In advance, this underestimation is expected to be enlarged as the amount of steel fiber is increased.

In order compare the differences in the post-cracking behavior according to changes in the amount of steel fiber in the concrete matrix and the compressive strength of concrete, another specimen (specimen 2) tested by Jungwirth and Muttoni (2004) was also selected. Its configuration and the material properties used in the experiment are shown in Fig. 11 and Table 2, respectively. Figs. 12 and 13 show results corresponding closely with those obtained in the previous specimen (specimen 1) have been obtained in spite of the relatively high compressive strength of concrete. An uncertain phenomenon is observed in Fig. 12; that is, the stiffness of member increases after steel yielding at

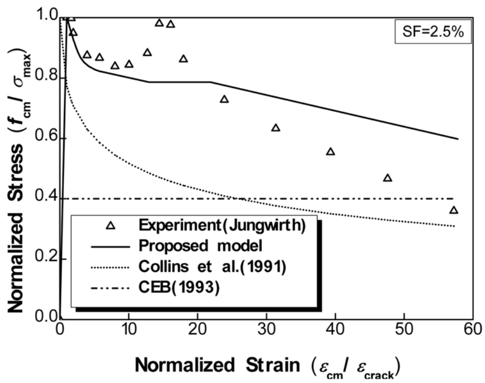

(a) 2.5 %

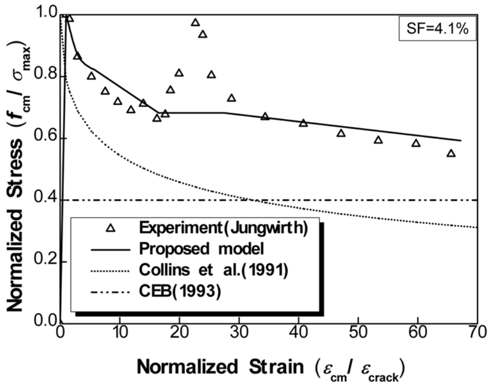

(b) 4.1 %

Fig. 12 Normalized stress-strain relationship

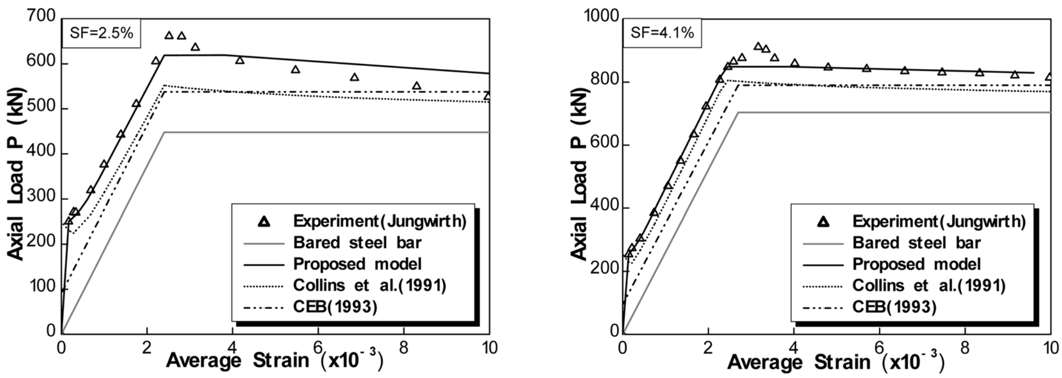

(a) 2.5 % (b) 4.1 %

Fig. 13 Member response with tension-stiffening effect

point B in Fig. 6. This phenomenon can be explained as the bridging effect of fiber after steel yielding at crack face. In spite of this phenomenon, the analytical results given by the introduced tension-stiffening model provide good agreement with the experimental results.

Finally, from the obtained results, it can be inferred that the introduced model can effectively simulate the tension-stiffening effect in a UHSFRC member regardless of changes in the compressive strength of concrete and the amount of steel fibers. Meanwhile, the direct use of the conventional relationship of normal strength reinforced concrete member leads to underestimation of the tension-stiffening effect even in the case of a UHSFRC member.

6. Numerical analysis

The experimental results from several UHSFRC beams tested at KICT (2005) were used to investigate the validity of the proposed analytical model. Because of a limited number of experimental data for UHSFRC members, in this paper the correlation studies between the analytical results and the experimental values have not been extended to various structural members beyond UHSFRC beams.

Four types of simply supported UHSFRC beams have been investigated as shown in Fig. 14. Each beam has a rectangular cross section size of $b \times h = 125\text{ mm} \times 250\text{ mm}$ and is reinforced with two mild steel bars. Two equal point loads are applied and their position is the major difference in each specimen (see Table 3). In advance, the same material properties of concrete and steel as those in the experimental study are used as follows: the yield strength of steel is $f_y = 538\text{ MPa}$, the elastic modulus of

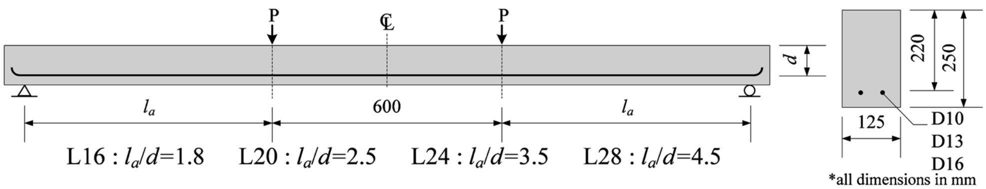

Fig. 14 Configuration of specimens

Table 3 Steel amounts and loading points

Specimen	D10L16	D10L20	D10L24	D10L28	D13L24
A_s	2D10	2D10	2D10	2D10	2D13
l_a (mm)	396	550	770	990	770
span ratio (l_a/d)	1.8	2.5	3.5	4.5	3.5

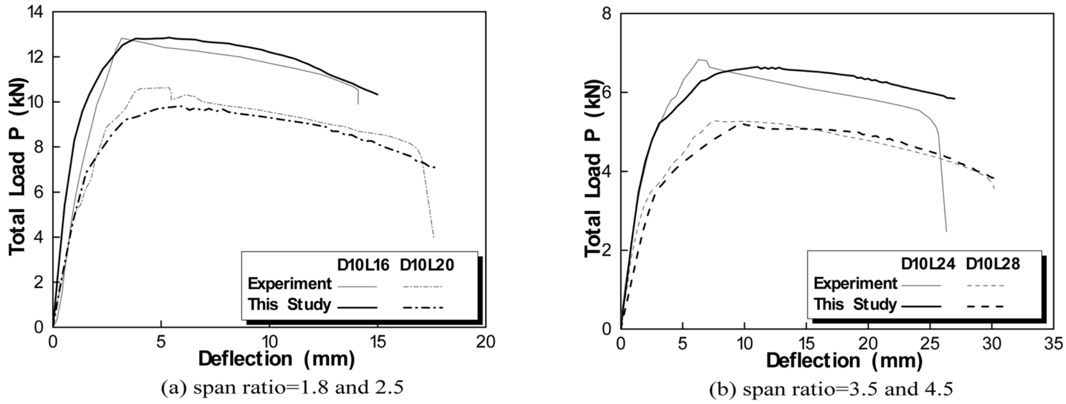

Fig. 15 Load-deflection relationships according to span ratio

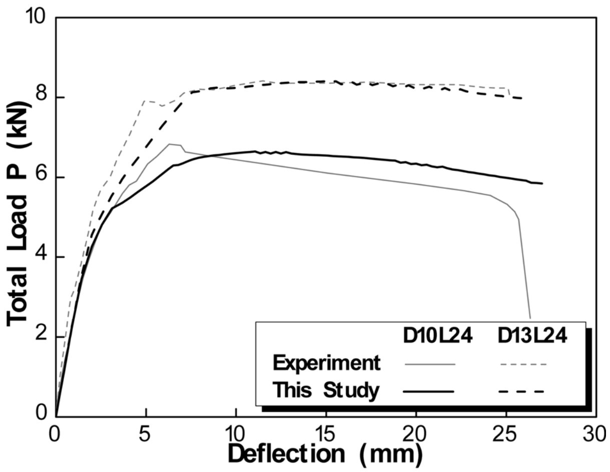

Fig. 16 Load-deflection relationships according to steel ratio

steel is $E_s = 200,000$ MPa, the compressive and the tensile strength of UHSFRC are $f_c' = 146$ MPa and $f_t = 13.9$ MPa, respectively, and the elastic modulus of concrete is $E_c = 49,000$ MPa. Uniform steel fiber of 2% is adopted for all specimens.

Fig. 15 represents a typical relationship between the applied lateral load and the corresponding vertical deflection at the mid-span according to the span ratio. The proposed numerical model not only gives accurate predictions for the ultimate load but also effectively simulates the nonlinear behavior of UHSFRC beams as the lateral load increases from zero to its ultimate value. All the specimens represented the bending failure, and Fig. 15 shows that an increase of the shear span ratio of l_a/d accompanies a decrease of the ultimate resisting capacity with an increase of the lateral deflection.

As the steel ratio increases, the ultimate capacity increases beyond steel yielding stress without major changes of the neutral axis of the section. The experimental data in Fig. 16 reflects more ductile behavior in specimen D13L24 in spite of having a larger steel ratio than specimen D10L24. This appears to be induced from ultimate resisting capacities and the post-yielding behavior in these specimens being governed by the concrete matrix in the tensile region rather than the yielding of the reinforcing bars.

In order to investigate the contribution of the tension-stiffening effect to the structural response,

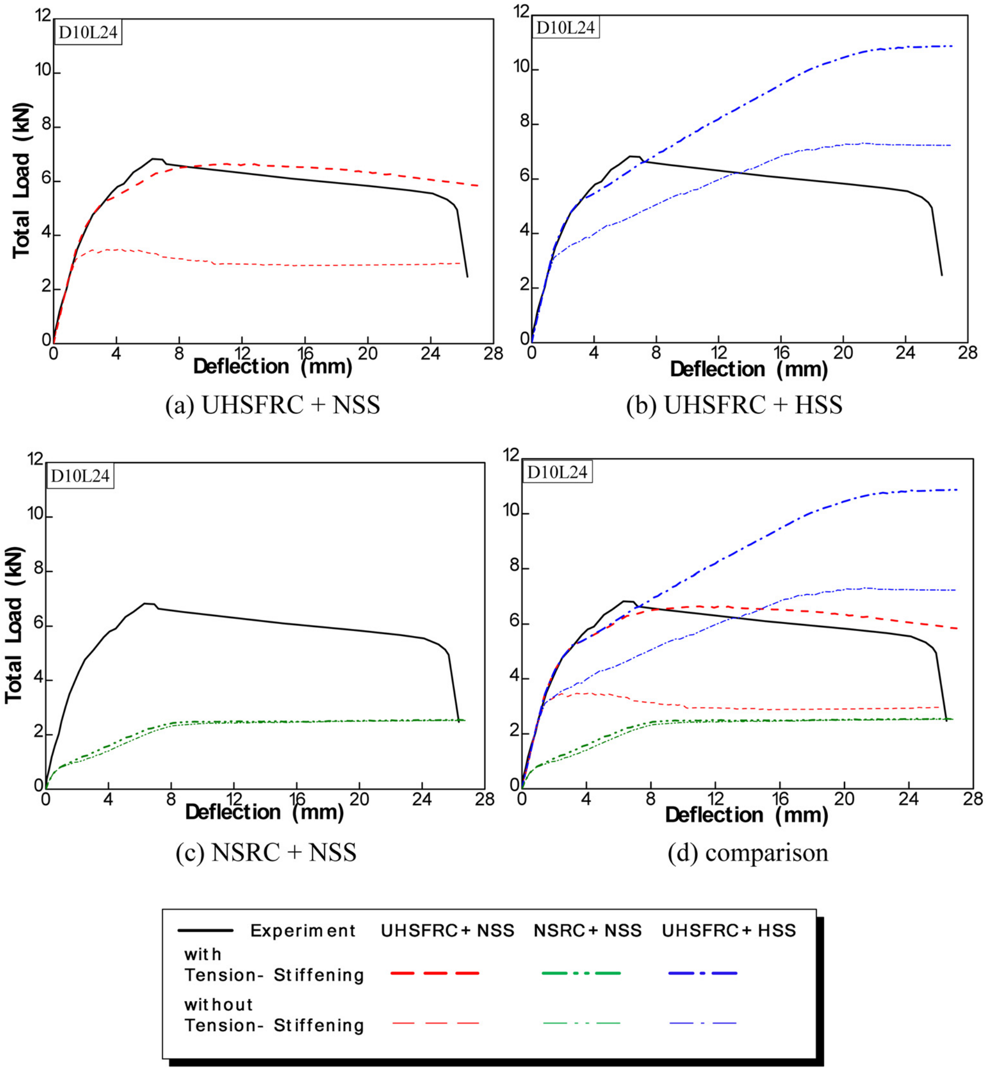

(e) legend

Fig. 17 Load-deflection relationships of specimen D10L24

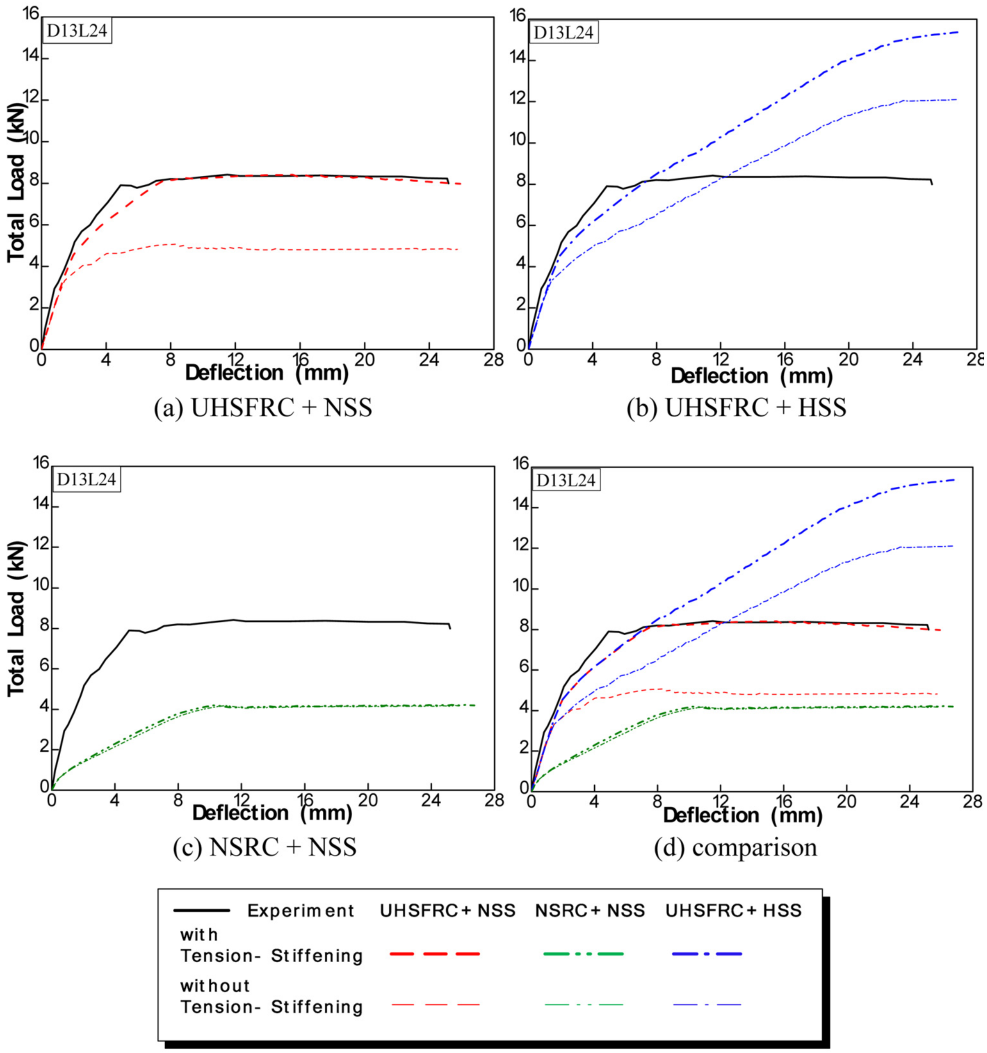

(e) legend

Fig. 18 Load-deflection relationships of specimen D13L24

analytical results with and without tension-stiffening are compared for two representative specimens, D10L24 and D13L24, in conjunction with changes in the compressive strength of concrete and the yield strength of steel. These two specimens present typical brittle and ductile behavior, respectively. For parametric studies, different strengths of materials from those used in the experiment are considered, and attention is given to normal strength concrete (NSC) with $f_c' = 40$ MPa and $f_t = 2.1$ MPa, ultra high strength concrete (UHSC) with $f_c' = 146$ MPa and $f_t = 13.9$ MPa, normal strength steel (NSS) with $f_y = 538$ MPa and high strength steel (HSS) with $f_y = 1,538$ MPa.

Figs. 17 and 18, which show the obtained results, lead to the following conclusions: (1) the tension-stiffening effect in the NSC beam (NSRC), representing the bending behavior, is not large enough to change the resisting capacity of the member (see Figs. 17(c) and 18(c)); (2) the entire structural behavior of the UHSFRC beam (UHSFRC), from the initial cracking to reach the ultimate resisting capacity, is dominantly governed by the tension-stiffening effect regardless of the change in steel strength. This large contribution of the tension-stiffening effect is induced from the bond effect between the steel fibers and the concrete matrix; (3) the structural response of specimen D10L24 is changed to ductile behavior when the reinforcing steel is changed from normal strength steel (NSS) to high strength steel (HSS). This means that the use of NSS is inappropriate with respect to ensuring ductility in UHSFRC beams; accordingly, (4) HSS must be used in the case of UHSFRC members for more rational design; (5) as shown in Figs. 17(a) and 18(a), when the tension-stiffening effect is not taken into account in the numerical simulation, the ultimate loads of UHSFRC case for both specimens D10L24 and D13L24 are almost the same as those of NSRC case, because the magnitude of the ultimate resisting capacity is directly proportional to the amount of reinforcing steel, and the equality between the developed moment by $M_u = P \cdot a/2$ and the sectional resisting capacity gives similar ultimate loads for both specimens. This phenomenon appears even when different materials are used (see Figs. 17(b) and 18(b) for the use of HSS and Figs. 17(c) and 18(c) for the use of NSC, respectively); and finally, (6) in order to exactly evaluate the ultimate resisting capacity of UHSFRC beams, the tension-stiffening effect derived on the basis of the mechanical behavior of UHSFRC must be considered in the numerical simulation.

7. Conclusions

In this paper, a numerical tension-stiffening model that can simulate the post-cracking behavior of UHSFRC members is proposed on the basis of the force equilibriums, compatibility conditions, and bond stress-slip relationship between the reinforcing steel and the surrounding concrete. In advance, the bond characteristics between the steel fibers and the concrete matrix are also taken into consideration, and the efficiency of the proposed model in finite element analyses is verified by comparison with reliable experimental results for UHSFRC beams.

Based on the results of limited correlation studies among the analytical results, the test values, and associated parametric studies, the following conclusions are obtained: (1) in order to exactly evaluate the ultimate resisting capacity of UHSFRC beams, the tension-stiffening effect must be considered; (2) in defining the tension-stiffening effect for UHSFRC structures, the bond characteristics between the concrete matrix and the embedded steel fibers must be incorporated; (3) the use of high strength steel are recommended in UHSFRC members in order to effectively use the enlarged resisting capacity of UHSFRC for tensile stress; and (4) the introduced tension-stiffening model can effectively be used in evaluating the ultimate resisting capacity of UHSFRC beam structures.

Acknowledgments

The work presented in this paper was funded by Center for Concrete Corea (05-CCT-D11), supported by Korea Institute of Construction and Transportation Technology Evaluation and Planning (KICTTEP) under the Ministry of Land, Transport and Maritime Affairs.

References

Attard, M.M. and Setunge, S. (1996), “Stress-strain relationship of confined and unconfined concrete”, *ACI Mater. J.*, **93**(5), 1-11.

Bischoff, P.H. (2003), “Tension-stiffening and cracking of steel fiber-reinforced concrete”, *J. Mater. Civil. Eng. - ASCE*, **15**(2), 174-182.

CEB-FIP (1993), *CEB-FIP model code 1990: design code*, CEB Bulletin d'Information No.213/214, Thomas Telford, London.

Collins, M.P. and Mitchell, D. (1991), *Prestressed concrete structures*, Prentice-Hall, Englewood Cliffs, NJ.

Crisfield, M.A. (1991), *Non-linear finite element analysis of solids and structures*, John Wiley and Sons, London.

Demeke, A. and Tegos, I.A. (1994), “Steel fiber reinforced concrete in biaxial stress tension-compression conditions”, *ACI Struct. J.*, **91**(5), 579-584.

Ezeldin, A.S. and Balaguru. P.N. (1992), “Normal- and high-strength fiber reinforced concrete under compression”, *J. J. Mater. Civil. Eng. - ASCE,* **4**(4), 415-429.

Fields, K. and Bischoff, P.H. (2004), “Tension-stiffening and cracking of high-strength reinforced concrete tension members”, *ACI Struct. J.*, **101**(4), 447-456.

Foster, S.J., Voo, Y.L. and Chong, K.T. (2006), “FE analysis of steel fiber reinforced concrete beams failing in shear: variable engagement model”, *ACI Special Public.*, **237**, 55-70.

Graybeal, B.A. (2007), “Compressive behavior of ultra-high-performance fiber-reinforced concrete”, *ACI Mater. J.*, **104**(2), 146-152.

Gupta, A.K. and Maestrini, S.R. (1990), “Tension-stiffness model for reinforced concrete bars”, *J. Struct. Eng. - ASCE,* **116**(3), 769-790.

Hognestad, E. (1951), *A study on combined bending and axial load in reinforced concrete members*, Bulletin Series No. 399, Bulletin No. 1., Engineering Experiment Station, University of Illinois, IL.

Hussein, A. and Marzouk, H. (2000), “Behavior of high-strength concrete under biaxial stresses”, *ACI Mater. J.*, **97**(1), 27-36.

Jungwirth, J. and Muttoni, A. (2004), “Structural behavior of tension members in UHPC”, *Proceeding of International Symposium on UHPC.*

Kölle, B., Phillips, D.V., Zhang, B., Bhatt, B. and Pearce, C.J. (2004), “Experimental investigation of the biaxial properties of high performance steel fibre reinforced concrete”, *Proceeding of 6th RILEM Symposium on Fibre-Reinforced Concrete (FRC): RILEM*, Varenna, Italy.

Korea Institute of Construction Technology (2005), *Development of girder using ultra-high performance cementitious composite for bridge*, KICTEP, Korea.

Kupfer, H., Hilsdorf, H.K. and Rusch, H. (1969), “Behavior of concrete under biaxial stresses”, *ACI J.,* **66(**8), 656-666.

Kwak, H.G. and Kim, D.Y. (2001), “Nonlinear analysis of RC shear walls considering tension-stiffening effect”, *Comp. Struct.*, **79**(5), 499-517.

Kwak, H.G. and Kim, D.Y. (2004), “Material nonlinear analysis of RC shear walls subject to monotonic loading”, *Eng. Struct.*, **26**(11), 1517-1533.

Kwak, H.G. and Na, C.K. (2007), “Nonlinear analysis of RC structures considering bond-slip effect”, *Korean Soc. Civil Eng*., **27**(3), 401-412.

Li, V.C. (1998), *Engineered cementitious composites-tailored composites through micromechanical modeling*, Canadian Society for Civil Engineering, Montreal.

Lorrain, M., Maurel, O. and Seffo, M. (1998), “Cracking behavior of reinforced high-strength concrete tension ties”, *ACI Struct. J.*, **95**(5), 626-635.

Mansur, M.A., Chin, M.S. and Wee, T.H. (1999), “Stress-strain relationship of high-strength fiber concrete in compression”, *J. Mater. Civil. Eng. - ASCE*, **11**(1), 21-29.

Redaelli, D. (2006), “Testing of reinforced high performance fibre concrete members in tension”, *Proceeding of 6th International Ph.D. Symposium in Civil Engineering*.

Rizkalla, S.H. and Hwang, L.S. (1984), “Crack prediction for members in uniaxial tension”, *ACI J.,* **81**(6), 572-579.

SETRA (2002), *Béntons Fibrés á Ultra-Hautes Peformances, Recommandations Provisoires*, Documents Scientifiques et Techniques, SETRA-AFGC, France.